Supporting Information

Area Negative Thermal Expansion in a Beryllium Borate $LiBeBO_3$ with Edge Sharing Tetrahedra

Wenjiao Yao[a, d, ‡], Xingxing Jiang[a, d, ‡], Rongjin Huang[*b], Wei Li[c], Chuanjun Huang [b], Zheshuai Lin[*a], Laifeng Li[b] and Chuangtian Chen[a]

[a] Beijing Center for Crystal R&D, Key Lab of Functional Crystals and Laser Technology, Technical Institute of Physics and Chemistry (TIPC), Chinese Academy of Sciences (CAS), Beijing 100190, PR China.

[b] Key Laboratory of Cryogenics, TIPC, CAS, Beijing, 100190, PR China

[c] Department of Materials Science and Metallurgy, University of Cambridge, Cambridge CB3 0FS, UK

[d] University of Chinese Academy of Sciences, Beijing 100049, PR China.

Corresponding Author

* Prof. Z. Lin, e-mail: zslin@mail.ipc.ac.cn

* Dr. R. Huang, email: huangrongjin@mail.ipc.ac.cn

Table of Content

1 Experimental Section

1.1 Synthesis and Crystal growth:

Li_2CO_3(AR), NaCl(AR), BeO (99.5%), H_3BO_3 (AR), B_2O_3(99.5%), and LiF (AR) from commercial sources were used as received. Platinum crucible was used as container for its stability and inertness even at high temperature. Owing to the toxicity of BeO, all of the experiments were performed in a ventilated system. The temperature was controlled with precision 0.1 K. Single and poly crystalline samples were obtained through spontaneous crystallization and traditional solid-state reaction, respectively.

In spontaneous crystallization, $LiBeBO_3$ single crystal was obtained with a molten flux based on LiF-BeO-B_2O_3-NaCl system in the molar ratio of 3:1:2.5:1. The initial goal product was sodium berylloborate chloride, which was supposed to have at least the similar ultraviolet absorption edge as sodium berylloborate, and LiF was meant to be an additive to improve viscosity. The raw materials at appropriate proportions were homogeneous mixed and placed in a platinum crucible and gradually heated to melt in a self-made furnace. The melt were kept at that temperature for at least 24 h with several stirs to ensure homogeneous. The temperature was then lowered at a rate of 10K per day until the mixture was curdled and to the room temperature in two days. Many colorless, transparent block crystals were obtained for later tests.

In solid state reaction, a stoichiometric mixture of Li_2CO_3, BeO and H_3BO_3 was carefully ground and mixed in an agate mortar and packed into a platinum crucible, which were then heated in a muffle furnace to about 600 K in the first round to ensure the decomposition of H_3BO_3 and Li_2CO_3. The mixture was ground adequately and heated gradually to 1000K for 2 days with several interval grindings until powder X-ray diffraction (PXRD) analyses display no changes.

The inductively coupled plasma (ICP) test revealed the molar ratio of Li:Be:B is 1:0.975:1.053.

1.2 Thermal analysis

Thermal behaviour of the compound was detected through differential scanning calorimetric measurements on grounded crystals of the title compound using a Labsys TG-DTA16 (SETARAM) thermal analyser calibrated with Al_2O_3. A sample (about 10 mg) of grounded crystal was placed in a platinum crucible and heated from room temperature to 900 ^oC at a rate of 10 ^oC /min in nitrogen atmosphere. The melted residues were examined and analysed by X-ray powder diffraction after the experiments.

1.3 Raman and IR spectra

The Raman pattern was recorded from 100 to 2000 cm^{-1} at room temperature, using in Via-Reflex, equipped with a solid state laser with a wavelength of 532 nm. In order to improve the signal to noise ratio of the spectra, 10 integrations were carried out on polycrystalline samples with an integration time of 10 s at a nominal resolution of 1 cm^{-1} and a precision of 1 cm^{-1}. The mid-infrared spectrum was obtained at room temperature in a range from 400 to 4000 cm^{-1} with resolution of 1 cm^{-1} via a Bio-Rad FTS-60 FTIR spectrometer. The sample and dried KBr (5 mg of the sample, 500 mg of KBr) were mixed thoroughly together.

1.4 Variable-temperature X-ray powder diffraction (VT-XRD)

The variable-temperature X-ray powder diffraction was recorded on finely grounded polycrystallines with a Bruker D8−discover X-ray diffractometer. Patterns in low (13-273K, at the interval of 20 K) and high temperature(298-848K, at the interval of 50 K) were written separately. The low-temperature condition was obtained by a G-M refrigerator, in which helium acts as the refrigerating fluid and the high-temperature condition was obtained by a high-precision high-temperature furnace.. The detailed parameters of X-ray were: Cu K*a* radiation (λ = 1.5418 Å); 40 kV; 30 mA; 2 mm divergence slit; 0.6 mm anti-scatter slit; 0.2 mm receiving slit; monochromatic; 0.1 mm detector slit; scanning step width of 0.01^o;

scanning rate of 0.5°/s; angular range 10° to 80°. The lattice parameters were refined by Rietveld method, using general structural analysis system (GSAS) software.

1.5 UV-Vis-NIR diffuse-reflectance pattern:

Data for the title compound were collected with a SolidSpec-3700 deep UV spectrophotometer in the wavelength range from 200 to 2500 nm. Fluororesin is applied as the standard.

1.6 First –principles calculations

The geometry optimization and vibrational spectra calculations were performed by CASTEP,[1] a plane-wave pseudopotential total energy package based on density functional theory (DFT).[2] The functional developed by Ceperley, Alder Perdew and Zunger (CA-PZ) in local density approximation (LDA)[3] form were adopted to search the minimum of the electron energy. The optimized norm-conserving pseudopential[4] in Kleiman-Bylander[5] form for Li, Be, B and O allow us to use a small plane basis set without compromising the accuracy required by the calculation. Kinetic energy cutoff of 900 eV and Monkhorst-pack[6] *k*-point mesh spanning less than 0.03 $Å^{-1}$ in the Brillouin zone were chosen. The Broyden–Fletcher–Goldfarb–Shanno (BFGS) minimization scheme[7] was employed and the convergence criteria for the structure optimization were set to 5.0×10^{-5} eV/atom, 0.1 eV/Å, 0.2 GPa and 5.0×10^{-3} GPa for energy, maximum force, maximum stress and maximum displacement, respectively. Based on crystal configuration in the minimal energy, the Raman and IR spectra were calculated by linear response formalism, in which the Raman and IR spectra were obtained by the second derivative of the total energy with respect to a given perturbation. Our tests showed that the above computational parameters and methodology are sufficiently accurate for current study.

2 Figure S1. Edge-sharing [Be_2O_6] group (a) Schematic diagram, (b) Charge-density difference in the planes of Be_2O_2 parallelogram (left) and O-Be-O dendrite (right). The Mulliken population for the chemical bonds d_1 (d_2) and d_3 (d_4) are 0.34 (0.39) and 0.55 (0.54), respectively, indicating the weaker covalent interaction in the former.

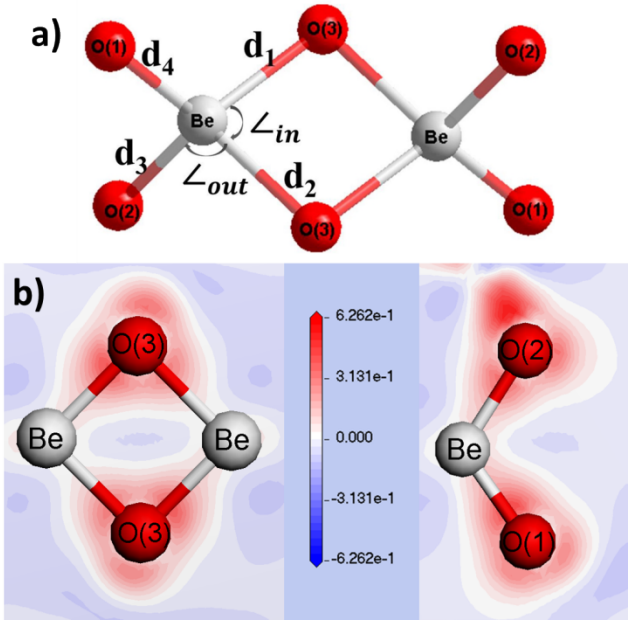

3 Figure S2. Stability of the $LiBeBO_3$ (a) thermal differential scanning curve (b) In situ powder XRD patterns from 13 K to 848 K.

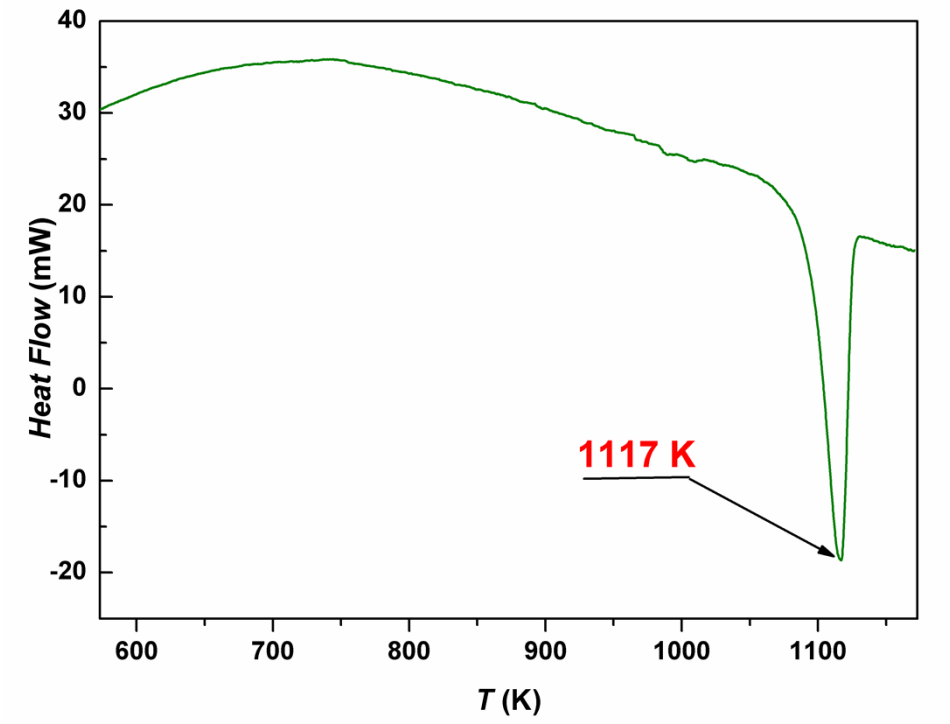

(a) Thermal differential scanning curve

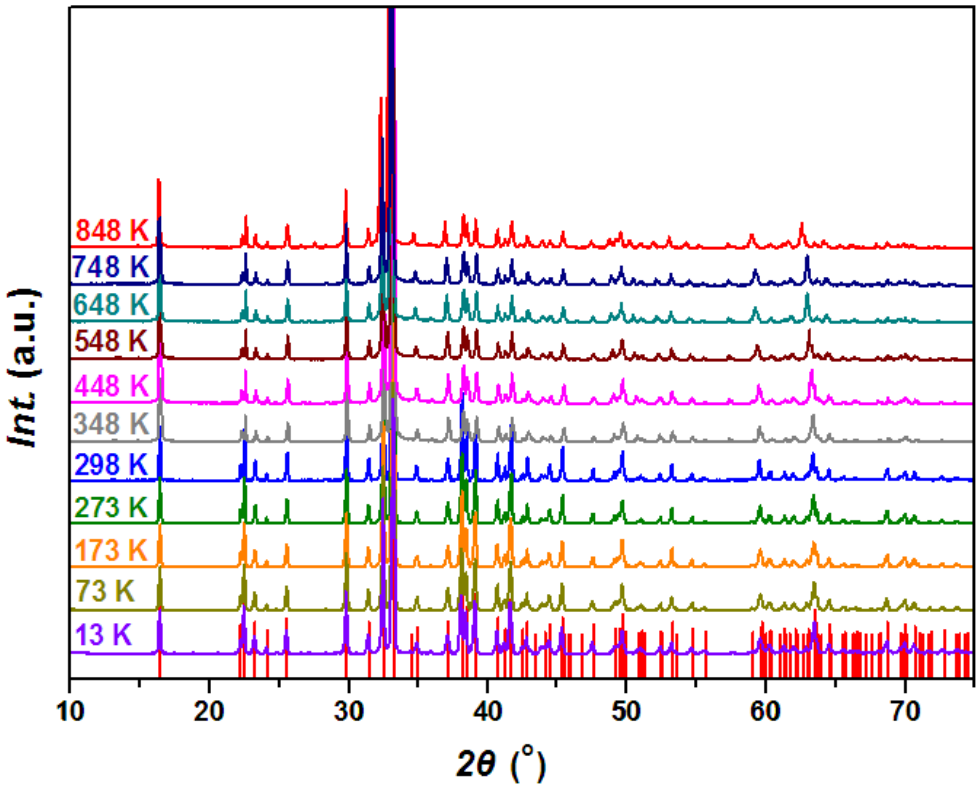

(b) In situ powder XRD patterns from 13 K to 848 K. Some for intercal temperature are removed for clarity of the plot.

4 Stability analyses based on the first-principles calculations

The [Be_2O_6] structure with a Be_2O_2 parallelogram and two O–Be–O dendrites formed by two edge-sharing BeO_4 tetrahedra in LBBO, as shown in Figure S1(a), is in confliction with the third Pauling's rule. As a common rule, the like-charges repulsion will push ions apart in the edge-sharing polyhedra to minimize electrostatic potential, thus the Be–O bond lengths within the parallelogram (d_1 and d_2) are elongated compared with those in the dendrites (d_3 and d_4). Meanwhile, the O–Be–O angles within the Be_2O_2 parallelogram ($\angle_{in}$) are prominently reduced by 15-20^o from the ideal value of 109.47° in a regular tetrahedron, while the $\angle_{out}$ is much closer to the average values observed in other beryllium borates.[8-13] This configuration might be essential to balance the electrostatic potential and maintain the geometric stability.

To further investigate the structural stability of the LBBO crystal, the first-principles atomic vibration analysis was performed. In the phonon spectrum, none of the imaginary phonon modes is observed. Meanwhile, the calculated IR and Raman spectra, which are in good agreement with the experimental results (Table S1), show that the optical peaks from the vibrational frequencies of edge-sharing BeO_4 tetrahedra are located in the high-frequency region and far from the imaginary region (Table S1). All these phonon-associated studies demonstrate that the including of edge-sharing BeO_4 tetrahedra in LBBO is dynamically stable. [14]

We further calculated the total energy of the LBBO structure and those of other existing compounds Li$M$$BO_3$ (M = Ca, Sr, Ba, Cd, Mn) with the M^{2+} cations hypothetically substituted by the Be^{2+} cations. The comparison shows that the LBBO structure has the lowest total energy (Table S2), demonstrating that this compound is energetically favorable to retain its structural novelty rather than to adopt other structures. Furthermore, the charge-difference analysis was employed to investigate the characteristics of chemical bonds[15] in the [Be_2O_6] group. As shown in Figure S1b, the electronic charges are accumulated between Be and O atoms, forming strong chemical bonds. However, the charge transfer inside the Be–O bonds in the Be_2O_2 parallelogram is smaller than that in the O–Be–O dendrites due to the lower bond order.

5 **Figure S3 Experimental IR and Raman spectrum**

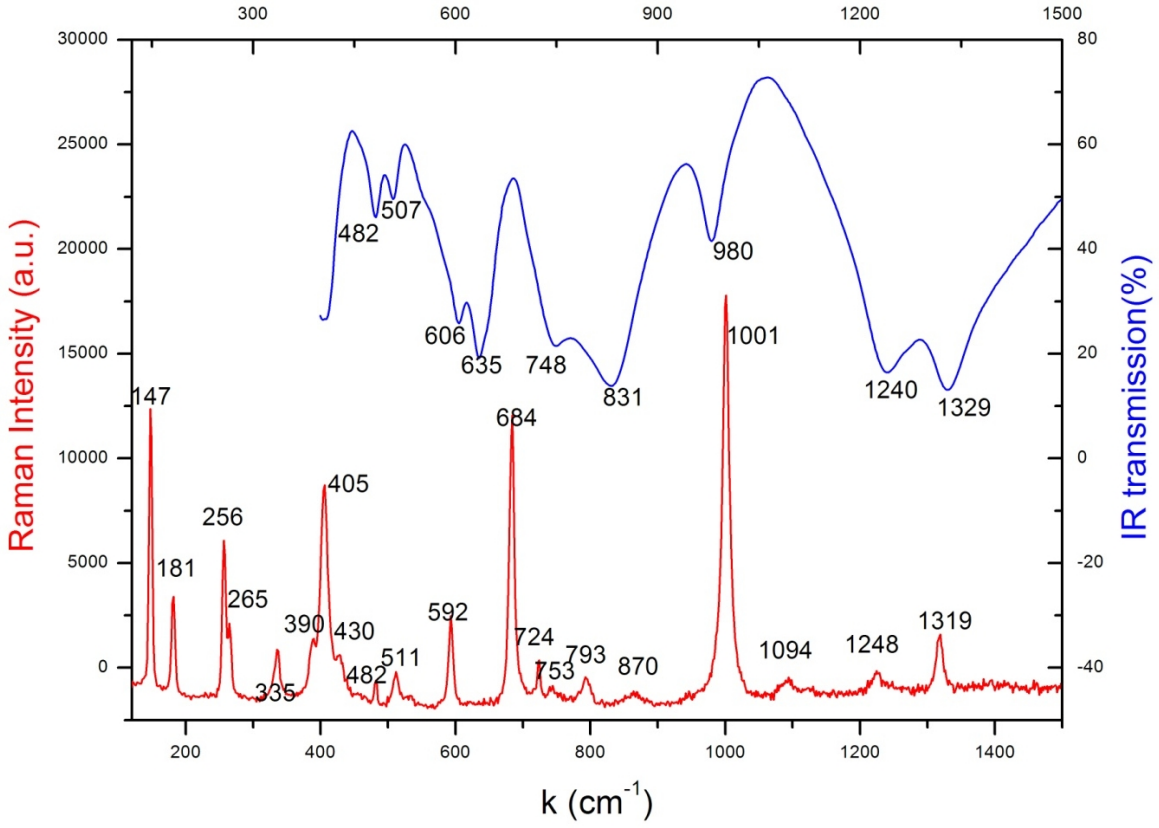

6 Table S1 The detailed assignments of atomic vibrations for the experimental IR and Raman optical modes by the first-principles calculations.

Exp. 298 K (cm^{-1})	Cal. 73 K (cm^{-1})	Cal. 193 K (cm^{-1})	Shift	Mode	Vibration assignment
147	144.596139	144.12522	0.470919	Bu	Be_2O_2 rotation
181	176.816731	176.427249	0.389482	Bu	BeO_4 rotation
	203.368338	203.499966	-0.131628	Ag	Li^+ in a unit cell to the same direction and BO_3 swing
	222.871334	222.90289	-0.031556	Bu	Li^+ in a unit cell to the opposite directions and Be_2O_2 stretching
256	248.964466	249.046214	-0.081748	Bu	BeO_4 stretching and BO_3 rotation
	280.629557	280.432538	0.197019	Ag	Li^+ in a unit cell to the opposite directions
	288.615428	288.625063	-0.009635	Bu	Li^+ in a unit cell to the same direction
	311.81991	311.570754	0.249156	Ag	BO_3 rotation and BeO_4 bending
	350.824063	350.815845	0.008218	Ag	Li^+ in a unit cell to the same direction
355	362.003028	361.889797	0.113231	Bu	Li^+ in a unit cell to the opposite directions
390	368.691036	368.759342	-0.068306	Bu	Be_2O_2 stretching and rotation, BO_3 swing
405	402.25107	401.573703	0.677367	Bu	BeO_4 stretching, Be_2O_2 bending and BO_3 rotation
	432.832606	432.977493	-0.144887	Ag	Li^+ in a unit cell to the same direction
	456.018816	456.055164	-0.036348	Ag	Li^+ in a unit cell to the same direction
482	470.246371	470.588258	-0.341887	Bu	Li^+ in a unit cell to the opposite directions
511	528.168657	528.086893	0.081764	Bu	BeO_4 stretching
	558.275053	558.275097	-4.4E-05	Bu	BeO_4 bending and stretching
	563.47336	563.878283	-0.404923	Ag	Be_2O_2 bending and BO_3 bending
606	581.391377	581.259556	0.131821	Ag	Be_2O_2 stretching
635	632.529928	632.529807	0.000121	Ag	Be_2O_2 and BO_3 stretching
648	636.501738	636.615582	-0.113844	Bu	Be_2O_2 stretching
	705.808537	705.775043	0.033494	Ag	BeO_4 bending and stretching
724	710.68165	710.884297	-0.202647	Bu	BeO_4 stretching
	728.651428	729.138248	-0.48682	Ag	Be_2O_2 stretching,
748	754.870441	754.978178	-0.107737	Bu	BO_3 bending

793	779.11873	779.484633	-0.365903	Ag	BeO_4 stretching and bending, Be_2O_2 stretching
831	808.882422	809.281009	-0.398587	Bu	BeO_4 stretching and bending, Be_2O_2 stretching
980	939.015473	939.143605	-0.128132	Ag	Be_2O_2 stretching
1001	963.791874	963.891292	-0.099418	Bu	BO_3 stretching and Be_2O_2 stretching
1240	1238.270084	1238.255372	0.014712	Ag	BO_3 stretching
1248	1243.596038	1243.743023	-0.146985	Bu	BO_3 stretching
1319	1323.220189	1323.362811	-0.142622	Ag	BO_3 stretching
1329	1327.8279	1327.927851	-0.099951	Bu	BO_3 stretching

7 Table S2 Cell lattices and energies per chemical formula as Be^{2+} cations hypothetically replace the M^{2+} cations in $LiMBO_3$ structures (M=Ca, Sr, Ba, Cd, Mn), where the $LiMBO_3$ structures come from Inorganic Crystal Structural Database.[16]

		Be	Ca	Sr	Ba	Cd	Mn
Space Group		P-*1*	P*bca*	P$2_1/c$	P$2_1/c$	P-*6*	P-*6*
lattice parameters	*a* (Å)	4.487 (4.621)	8.478	7.282	4.668	7.491	7.492
	b (Å)	4.547 (4.678)	8.247	6.050	10.67	7.491	7.492
	c (Å)	5.666 (5.870)	6.181	4.621	5.187	2.614	2.615
	α (°)	67.91 (68.24)	90	90	90	90	90
	β (°)	72.37 (72.03)	90	88.75	127.05	90	90
	γ (°)	61.04 (61.08)	90	90	90	90	90
Energy per chemical formula (eV)		**-1407.92**	**-1406.58**	**-1406.57**	**-1316.40**	**-1404.33**	**-1405.22**

8 Table S3 The refined cell parameters of $LiBeBO_3$ under the temperature from 13 K to 273 K and from 298 K to 848 K.

T (K)	*a* (Å)	*b* (Å)	*c* (Å)	*α* (°)	*β* (°)	*γ* (°)	*Volumn*	*Area of ab plane*
13	4.62891(22)	4.68556(24)	5.87365(14)	68.2137(32)	72.0241(27)	61.0591(29)	102.209(5)	18.9804(27)
33	4.62892(22)	4.68552(24)	5.87384(14)	68.2152(32)	72.0250(27)	61.0592(29)	102.213(5)	18.9803(27)
53	4.62893(22)	4.68563(24)	5.8738(14)	68.2153(32)	72.0246(27)	61.0582(29)	102.214(5)	18.9806(27)
73	4.62897(22)	4.68561(24)	5.87367(14)	68.215(32)	72.0241(27)	61.0586(29)	102.212(5)	18.9808(26)
93	4.62886(22)	4.68552(24)	5.87386(14)	68.2161(32)	72.0260(27)	61.0581(29)	102.212(5)	18.9799(27)
113	4.62857(22)	4.68528(24)	5.87427(14)	68.2188(33)	72.0309(27)	61.0580(30)	102.210(5)	18.9777(27)
133	4.62825(22)	4.68507(24)	5.87484(14)	68.2208(33)	72.0354(28)	61.0581(30)	102.211(5)	18.9756(26)
153	4.62794(22)	4.68503(25)	5.87555(14)	68.2224(33)	72.0424(28)	61.0580(30)	102.219(5)	18.9741(27)
173	4.62761(23)	4.68474(25)	5.87659(14)	68.2266(34)	72.0483(28)	61.0580(30)	102.228(5)	18.9716(27)
193	4.62743(23)	4.68468(25)	5.87777(15)	68.2296(34)	72.0551(29)	61.0567(31)	102.246(5)	18.9704(26)
213	4.62724(24)	4.68471(26)	5.87916(15)	68.2333(35)	72.0639(30)	61.0581(33)	102.273(5)	18.9700(28)
233	4.62715(23)	4.68454(26)	5.88059(15)	68.2351(35)	72.0693(29)	61.0557(32)	102.293(5)	18.9685(28)
253	4.62713(24)	4.68480(26)	5.88240(15)	68.2367(35)	72.0766(29)	61.0546(32)	102.332(5)	18.9692(28)
273	4.62712(24)	4.68485(26)	5.88415(15)	68.2402(35)	72.0852(29)	61.0539(32)	102.368(5)	18.9693(28)
298	4.62145(18)	4.67917(19)	5.88034(11)	68.2164(26)	72.0918(22)	61.0569(24)	102.044(4)	18.9236(21)
348	4.62144(19)	4.67943(20)	5.88649(12)	68.2194(27)	72.1136(23)	61.0524(26)	102.161(4)	18.9238(21)
398	4.62180(20)	4.68000(21)	5.89304(13)	68.2189(29)	72.1312(24)	61.0486(27)	102.297(4)	18.9269(22)
448	4.62236(21)	4.68049(23)	5.89895(13)	68.2186(30)	72.1420(25)	61.0447(28)	102.423(4)	18.9305(23)
498	4.62299(22)	4.68101(24)	5.90464(14)	68.2172(32)	72.1485(27)	61.0408(30)	102.545(5)	18.9344(24)
548	4.62360(23)	4.68164(25)	5.91061(14)	68.2144(33)	72.1545(28)	61.0360(31)	102.672(5)	18.9360(25)
598	4.62435(25)	4.68226(27)	5.91664(15)	68.2113(35)	72.1555(29)	61.0288(33)	102.799(5)	18.9378(26)
648	4.62500(26)	4.68279(28)	5.92295(16)	68.207(4)	72.1531(31)	61.0198(35)	102.923(5)	18.9388(26)
698	4.62573(27)	4.68359(30)	5.92990(16)	68.198(4)	72.1470(33)	61.010(4)	103.061(6)	18.9400(27)
748	4.62661(28)	4.68450(31)	5.93718(17)	68.187(4)	72.1397(35)	60.998(4)	103.208(6)	18.9414(27)
798	4.62778(28)	4.68570(31)	5.94516(17)	68.175(4)	72.123(4)	60.989(4)	103.379(6)	18.9445(27)
848	4.62909(28)	4.68688(32)	5.95352(18)	68.162(4)	72.096(4)	60.976(4)	103.551(6)	

9 Table S4 The relationship between principal axes *X*, *Y*, *Z* and crystallographic axes *a*, *b*, *c*.

$$\begin{pmatrix} X \\ Y \\ Z \end{pmatrix} = \begin{pmatrix} 0.9092 & -0.4045 & 0.0953 \\ -0.0837 & 0.9957 & -0.0395 \\ -0.3626 & -0.2109 & 0.9078 \end{pmatrix} \begin{pmatrix} a \\ b \\ c \end{pmatrix}$$

10 The relationship between Grüneisen parameter and thermal expansion coefficient

The relationship between macroscopic Grüneisen parameter and thermal expansion coefficient is given as[17]

$$\alpha = \frac{C_v \rho}{K_T} \gamma \qquad \text{(a)}$$

where α is thermal expansion coefficient, C_v is the principle heat capacity,ρis density, K_T is isothermal bulk moduli, γ is thermacroscopic Grüneisen parameter. The macroscopic Grüneisen parameter is the sum of the microscopic Grüneisen parameter of the phonon model by weight, i.e.,

$$\gamma = \frac{\sum_i c_i \gamma_i}{\sum_i c_i} \qquad \text{(b)}$$

where c_i is the partial contribution to the heat capacity of vibrational mode i. And the microscopic Grüneisen parameter of an individual vibrational mode i can then be defined as (the negative of) the logarithmic derivative of the corresponding frequency ω_i:

$$\gamma_i = -\frac{V}{\omega_i} \frac{\partial \omega_i}{\partial V}$$

And V is the volume. So if the frequency of a vibration mode increases with the increasing volume (increasing temperature), it will contribute negatively to thermal expansion (NTE).

11 Table S5 The CSD numbers for the crystal information files at 73 K and 193 K

Temperature	73 K	193 K
CSD number	428431	428432

12 References

[1] S. J. Clark, M. D. Segall, C. J. Pickard, P. J. Hasnip, M. J. Probert, K. Refson, M. C. Payne, *Z. Kristallogr.* **2005,** *220* (5-6), 567-570.

[2] W. Kohn, L. J. Sham, *Phys. Rev.* **1965,** *140* (4A), 1133-&.

[3] a) D. M.Ceperley, B. J. Alder, *Phys. Rev. Lett.* **1980**, *45* (7), 566-569; b) J. P. Perdew, A. Zunger, *Phys. Rev. B* **1981**, *23* (10), 5048-5079.

[4] A. M. Rappe, K. M. Rabe, E. Kaxiras, J. D. Joannopoulos, *Phys. Rev. B* **1990**, *41* (2), 1227-1230.

[5] L. Kleinman, D. M. Bylander, *Phys. Rev. Lett.* **1982,** *48* (20), 1425-1428.

[6] H. J. Monkhorst, J. D. Pack, *Phys Rev B* **1976,** *13* (12), 5188-5192.

[7] B. G. Pfrommer, M. Cote, S. G. Louie, M. L. Cohen, *J. Compu. Phys.* **1997**, *131* (1), 233-240.

[8] C. T. Chen, Y. B. Wang, B. C. Wu, K. Wu, W. L. Zeng, L. H. Yu, *Nat.* **1995**, *373*, 322−324.

[9] a) H. W. Huang, J. Y. Yao, Z. S. Lin, X. Y. Wang, R. He, W. J. Yao, N. X. Zhai, C. T. Chen, *Angew. Chem. Int. Ed.* **2011**, *50*, 9141−9144; b) H. W. Huang, J. Y. Yao, Z. S. Lin, X. Y. Wang, R. He, W. J. Yao, N. X. Zhai, C. T. Chen, *Chem. Mater.* **2011**, *23*, 5457−5463.

[10] a) S. F. Jin, G. M. Cai, W. Y. Wang, M. He, S. C. Wang, X. L. Chen, *Angew. Chem. Int. Ed.* **2010**, *49*, 4967 –4970; b) J. K. Burdett, Timothy J. McLarnan, *J. Am. Chem. Soc.* **1982**, *104*, 5229-5230.

[11] S. C. Wang, N. Ye, W. Li, D. Zhao, *J. Am. Chem. Soc.* **2010**, *132*, 8779−8786.

[12] S. C. Wang, N. Ye, *J. Am. Chem. Soc.* **2011**, *133*, 11458–11461.

[13] H. W. Huang, L. J. Liu, S. F. Jin, W. J. Yao, Y. H. Zhang, C. T. Chen, *J. Am. Chem. Soc.* **2013**, *135*, 18319−18322.

[14] L. Yang, W. L. Fan, Y. L. Li, H. G. Sun, L. Wei, X. F. Cheng, X. Zhao, *Inorg. Chem.* **2012**, *51*, 6762−6770.

[15] P. Doz, D. Cremer, E. Kraka, *Angew. Chem. Int. Ed.* **1984**, *23*(8), 627–628.

[16] ICSD, 2012-1, Version 1.8.2, by Fachinformatiionszentrum Karlsruhe, Germany.

[17] G. D. Barrera, J. A. Bruno, T. H. K. Barron, N. L. Allan, *J. Phys.: Condens. Matter*, **2005**, *17*, 217–252.